



OPEN

Effect of Li⁺ doping on the luminescence performance of a novel KAlSiO₄:Tb³⁺ green-emitting phosphor

Reziwanguli Yantake^{1,2,3}, Muyasier Kaiheriman⁴, Taximaiti Yusufu^{1,2,3} & Aierken Sidike^{1,2,3}

A new green-emitting phosphor, KAlSiO₄:1.5 mol% Tb³⁺, *x* mol% Li⁺, was prepared via a high-temperature solid-phase method, and its crystal structure, diffuse reflectance spectrum, and luminescence were studied. The results show that the Li⁺ doping shifts the strongest diffraction peak to a high angle direction, reducing grain size by 11.4%. The entry of Li₂CO₃ improves the luminescence performance of KAlSiO₄:1.5 mol% Tb³⁺. At a Li⁺ concentration of 1.5 mol%, the sample has strong absorption in the ultraviolet light range from 250 to 400 nm. The luminous intensity of the sample at 550 nm approximately quadruples after Li⁺ doping. Additionally, the colour purity of the sample and the internal quantum yield increase to 83.3% and 42%, respectively. The sample changes colour with time when exposed to air without an obvious fading phenomenon. The emission intensity at 200 °C is 95.1% of its value at room temperature, indicating that the phosphor has excellent thermal stability when *x* = 1.5. These results show the feasibility of using the silicate phosphor for generating the green light component of white light-emitting diodes for solid-state lighting.

In recent years, rare earth luminescent materials have been widely used in white light-emitting diodes (w-LEDs) because of their long life and high efficiency¹. In commercial solid-state lighting, phosphor-converted LEDs (pc-WLEDs) offer many advantages including low cost, good colour rendering, high colour purity, and good chemical stability. pc-WLEDs have also attracted the attention of many researchers².

Silicate phosphor luminescent materials for LED lighting are made of cheap raw materials. They offer good thermal stability and have a long life. Muyasier et al. prepared a green Na₈Al₆Si₆O₂₄Cl₂: *x* mol% Tb³⁺ phosphor and analysed the luminescence spectrum and colour coordinates, and they found that the silicate phosphor has a lifetime of up to 2.8 ms with good thermal stability³. Wan et al. prepared BaAl₂Si₂O₈:Tb³⁺, Ce³⁺ phosphors, studied their photoluminescence characteristics, and found that they can be used as green phosphors⁴. Yu et al. prepared Sr₂SiO₄:Tb³⁺, Ce³⁺ phosphors with a lifetime of up to 2.85 ms. The colour of this phosphor can be changed from green to blue by using the high-temperature solid-phase method⁵. Dilare et al. prepared NaAlSi₃O₈:Tb³⁺ phosphor and obtained a new type of silicate luminescent material with tuneable colours from green to red⁶. KAlSiO₄ has potential applications in luminescent glass and optical devices. In recent years, a few groups have reported on artificially synthesised KAlSiO₄ doped with other rare earths to prepare three-color phosphors suitable for white LEDs.

Since Tb³⁺ has a strong green emission band in the wavelength range of 535 nm–555 nm, rare earth luminescent materials doped with Tb³⁺ can often be used to obtain the green component of an ideal white LED⁷. The actual luminous intensity of Tb³⁺ is generally determined by the crystal field coordination environment in the selected matrix. When different valencies are substituted, Li⁺ can often be used as a charge compensator or a flux to achieve the desired luminous efficiency. Li Zhen et al. reported a new green emitting phosphor Sr₂MgB₂O₆:Tb³⁺, *x* mol% Li⁺ with good thermal stability and a maximum doping concentration of 9 mol%⁸. Potassium aluminosilicate (KAlSiO₄) has a lattice site suitable for rare earth doping, and the corresponding crystal symmetry is relatively high. The standard card number of this material is 33–0989. In this study, a new type of green-emitting phosphor, KAlSiO₄: 1.5 mol% Tb³⁺, *x* mol% Li⁺, was synthesised by a high-temperature

¹College of Physics and Electronic Engineering, Xinjiang Normal University, Urumqi 830054, Xinjiang, China. ²Key Laboratory of Mineral Luminescent Material and Microstructure of Xinjiang, Urumqi 830054, Xinjiang, China. ³Key Laboratory of New Light Source and Micro-Nano Optics, Urumqi 830054, Xinjiang, China. ⁴Urumqi Campus of Army Academy of Border and Coastal Defense, Urumqi 830002, Xinjiang, China. ✉email: taxmammat_84@sina.com; aierkenjiang@sina.com

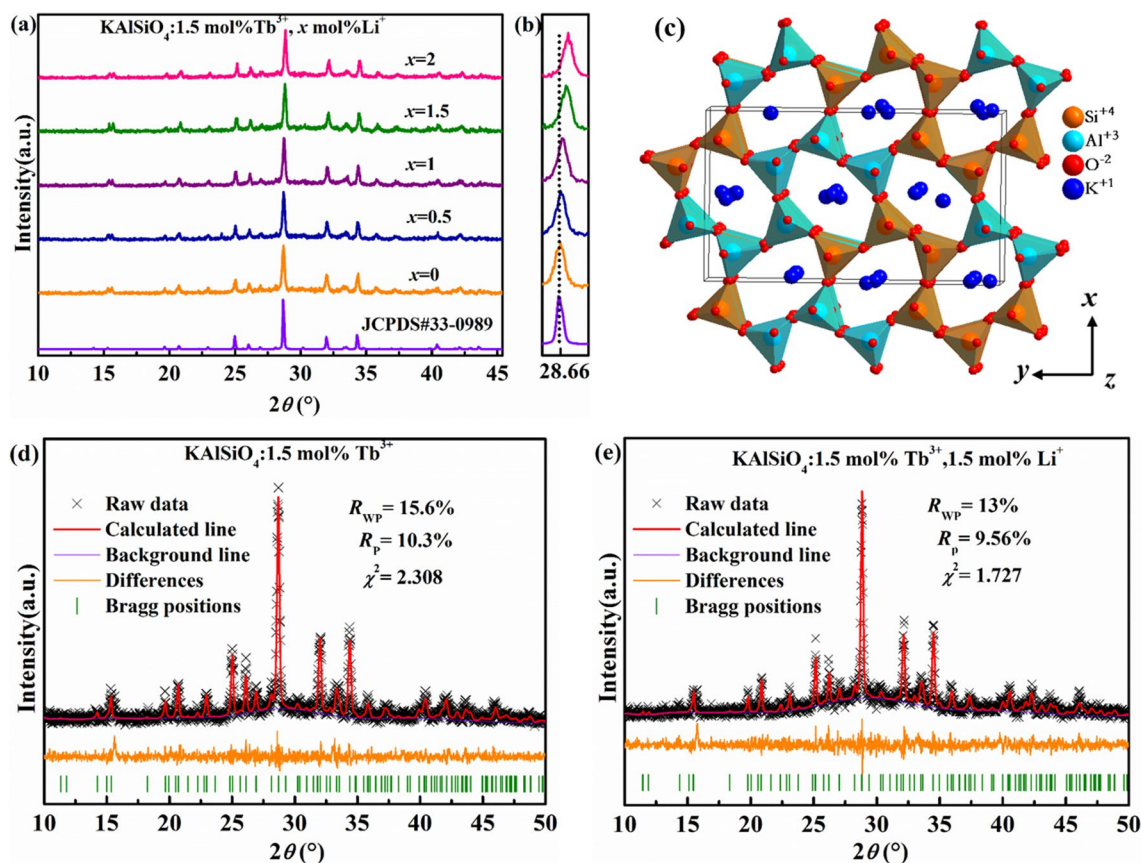


Figure 1. (a, b) X-ray diffraction pattern of $\text{KAlSiO}_4:1.5 \text{ mol\% Tb}^{3+}, x \text{ mol\% Li}^+$. (c) Crystal structure of KAlSiO_4 . (d) Refined XRD image of $\text{KAlSiO}_4:1.5 \text{ mol\% Tb}^{3+}$ and (e) $\text{KAlSiO}_4:1.5 \text{ mol\% Tb}^{3+}, 1.5 \text{ mol\% Li}^+$.

solid-phase method. The crystal structure, photoluminescence characteristics, UV–Vis absorption spectrum, colour coordinates, and colour purity of the samples were systematically studied. The addition of Li^+ improves the luminescence performance of $\text{KAlSiO}_4:1.5 \text{ mol\% Tb}^{3+}$, making it a new type of green silicate phosphor with potential application as the green component of white LEDs.

Experimental results and discussion

Phase analysis of $\text{KAlSiO}_4:1.5 \text{ mol\% Tb}^{3+}, x \text{ mol\% Li}^+$ series samples. Figure 1a shows the X-ray diffraction pattern of the $\text{KAlSiO}_4:1.5 \text{ mol\% Tb}^{3+}, x \text{ mol\% Li}^+$ ($x=0, 0.5, 1, 1.5, 2$) sample. It can be seen from the figure that the diffraction peaks are consistent with the standard JCPDS No. 33–0989. Figure 1b shows an enlarged view of the strongest diffraction peak at 28.66° . The peak appears to gradually shift to a high-angle direction. Both Li^+ and Tb^{3+} are added to the crystal lattice. It can be inferred that Li_2CO_3 can be used as a charge compensator in the KAlSiO_4 crystal lattice to adjust the valence state of ions to achieve charge balance¹. When $\text{CN}=7$, Tb^{3+} ($r=0.098 \text{ nm}$) and Li^+ ($r=0.092 \text{ nm}$) are close to the seven-coordinate K^+ radius ($r=0.146 \text{ nm}$) in KAlSiO_4 , whereas Si^{4+} ($r=0.026 \text{ nm}$) and Al^{3+} ($r=0.039 \text{ nm}$) have smaller radii. Hence, Tb^{3+} and Li^+ replace the K^+ positions. According to the Bragg formula [Eq. (1)]⁶, the interplanar spacing (d) will be reduced after the substitution. Hence, the diffraction peak position moves to a higher angle direction.

$$2d \sin \theta = n\lambda \quad (1)$$

where θ is the Bragg angle of X-ray diffraction peak, d is the interplanar spacing, n stands for constant factor, and λ represents the incident X-ray wavelength.

Figure 1c shows the crystal structure of KAlSiO_4 . There are many types of KAlSiO_4 space groups. The space group corresponding to KAlSiO_4 synthesised in this study is $\text{P}212121(19)$, which is an orthorhombic structure ($\alpha = \beta = \gamma = 90^\circ$) with unit cell parameters $a = 0.9057 \text{ nm}$, $b = 1.5642 \text{ nm}$, $c = 0.8582 \text{ nm}$, and $V = 1.2158 \text{ nm}^3$. It can be seen from the figure that K^+ is filled between the $[\text{SiO}_4]$ and $[\text{AlO}_4]$ tetrahedrons. K^+ has a 7-coordinated 4a site with higher symmetry and a 10-coordinated 4a site with lower symmetry in KAlSiO_4 crystals. The crystal structure along the z -axis has high symmetry. This is conducive to the narrowband emission of Tb^{3+} .

Figure 1d,e show the refined XRD images of $\text{KAlSiO}_4:1.5 \text{ mol\% Tb}^{3+}$ and $\text{KAlSiO}_4:1.5 \text{ mol\% Tb}^{3+}, 1.5 \text{ mol\% Li}^+$, respectively. It can be seen from the refined diagram that the XRD refined results of this series of samples are reliable. It was further confirmed that Tb^{3+} and Li^+ doping had no significant effect on the crystal structure of KAlSiO_4 .

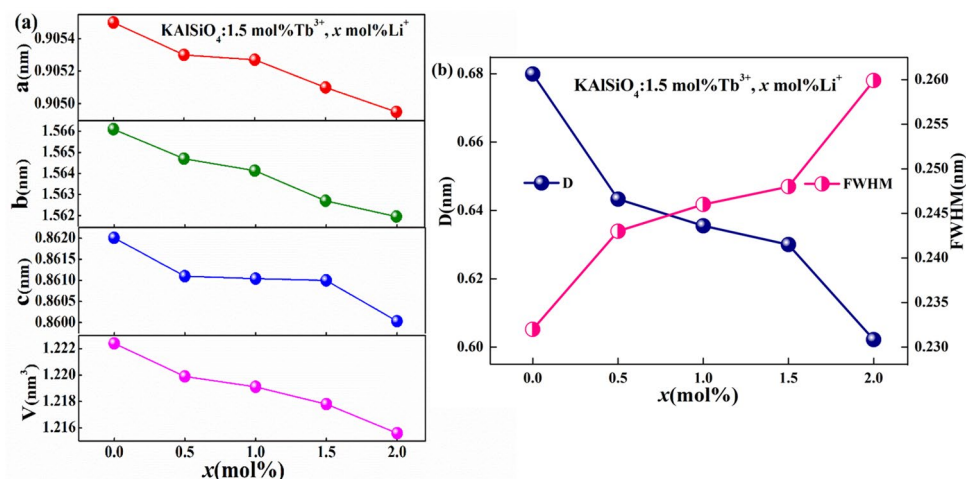


Figure 2. (a) Variation of the unit cell parameters with doping concentration ($x=0,0.5,1,1.5,2$) for $\text{KAlSiO}_4:1.5 \text{ mol\% Tb}^{3+}, x \text{ mol\% Li}^+$ (b) The relationship between x , the grain size, and the (202) crystal plane FWHM in $\text{KAlSiO}_4:1.5 \text{ mol\% Tb}^{3+}, x \text{ mol\% Li}^+$.

Figure 2a shows the variation of the unit cell parameters of $\text{KAlSiO}_4:1.5 \text{ mol\% Tb}^{3+}, x \text{ mol\% Li}^+$ for various doping concentrations ($x=0,0.5,1,1.5,2$). The changes in V , a , b , and c can be obtained from the refined XRD results. The relational formula [Eq. (2)]⁹ of the orthorhombic crystal plane spacing d (hkl) and crystal plane group (hkl) is used for the verification.

$$\frac{1}{d^2} = \frac{h^2}{a^2} + \frac{k^2}{b^2} + \frac{l^2}{c^2} \quad (2)$$

It can be seen from the figure that as the Li^+ concentration increases, the values of V , a , b , and c decrease to varying degrees. When Tb^{3+} and Li^+ , which have a small radius, replaces the large radius of K^+ , the volume of the unit cell will shrink, causing the unit cell parameters to gradually show a downward trend.

Figure 2b shows the relationship between x in $\text{KAlSiO}_4:1.5 \text{ mol\% Tb}^{3+}, x \text{ mol\% Li}^+$ ($x=0,0.5,1,1.5,2$), the grain size and the (202) full width at half maximum (FWHM) of the crystal plane. The grain size (D) is calculated using Eq. (3)^{10,11}.

$$D = \frac{K\lambda}{W \cos \theta} \quad (3)$$

Here, $\lambda=0.15406 \text{ nm}$ and $K=0.89$. W is the FWHM corresponding to the strongest diffraction peak, and θ is the angle of the strongest diffraction peak. With the increase in x , the grain size of the sample decreased by 11.4%, further confirming the shift of the XRD diffraction peak to the high-angle direction.

Luminescence characteristics of $\text{KAlSiO}_4: x \text{ mol\% Tb}^{3+}$ series samples. Figure 3 shows the excitation and emission spectra of the representative sample $\text{KAlSiO}_4:1.5 \text{ mol\% Tb}^{3+}$. The inset is an enlarged view of the excitation spectrum in the range from 325 to 425 nm. Under the excitation of the characteristic excitation wavelength of Tb^{3+} at 378 nm, it can be seen from the figure that the strongest emission peak of the phosphor is at 550 nm, which belongs to the narrow-band green light emission. The phenomenon of spectral splitting occurs at 540 nm. This is because the 7 coordination of Tb^{3+} is substituted. K^+ has a low symmetry position (Fig. 1c), which is affected by the crystal field environment. Compared with¹², the strongest emission peak has a blue shift of 5 nm. Under 550 nm monitoring, a charge transfer band appeared in the range from 200 to 300 nm. There are different excitation bands from 200–500 nm, indicating that the sample can be effectively excited by ultraviolet light. The charge transfer band (CTB) of Tb^{3+} ions at 249 nm is attributed to the $4f-5d$ transition of Tb^{3+} ion^{7,13}. Owing to the strong symmetry of potassium aluminosilicate belonging to the frame silicate series, the incorporated Tb^{3+} ions are less affected by the crystal field environment, and there is no obvious spectral split at 249 nm and 378 nm. When the sample was excited at 378 nm, it was found that the electrons in the 7F_6 ground state of Tb^{3+} in the sample were excited to the 5D_J ($J=2,3,4$) excited state. These electrons then relaxed to the 5D_4 energy level by non-radiative transition, while some of the electrons undergo 5D_4 to 7F_J ($J=6,5,4,3$) radiative transition¹⁴.

Figure 4 is a diagram of the concentration quenching mechanism of $\text{KAlSiO}_4:x \text{ mol\% Tb}^{3+}$ ($x=0.5,1,1.5,2$). It can be seen that when $x=1.5$, the absorption intensity at 378 nm in the excitation spectrum is the strongest, resulting in the strongest emission intensity. The luminous intensity of the sample reaches its maximum, and concentration quenching occurs. When the concentration was increased beyond 1.5 mol%, the absorption intensity of each peak began to decrease slightly. The critical distance is calculated using Eq. (4)¹⁵:

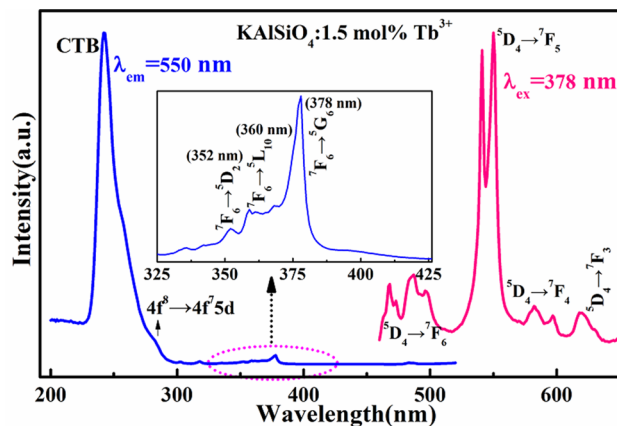


Figure 3. Excitation and emission spectra of $\text{KAlSiO}_4:1.5 \text{ mol\% Tb}^{3+}$ (the inset is an enlarged view of the excitation spectrum from 325–425 nm).

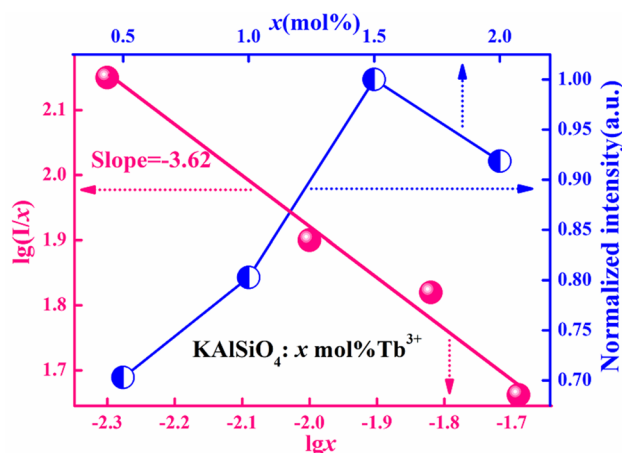


Figure 4. Concentration quenching mechanism diagram for $\text{KAlSiO}_4: x \text{ mol\% Tb}^{3+}$ ($x=0.5, 1, 1.5, 2$).

$$R_c = 2 \left(\frac{3V}{4\pi X_c N} \right)^{\frac{1}{3}} \quad (4)$$

R_c is the critical distance of concentration quenching, X_c is the critical concentration of Tb^{3+} , V is the unit cell volume, and N is the number of unit cells. In this series of samples, $V = 1.2158 \text{ nm}^3$, $X_c = 0.015$, and $N = 12$. It is concluded that $R_c = 2.35 \text{ nm}$, which is greater than 0.5 nm . (' 0.5 nm ' is an index that distinguishes exchange interaction and electrical multi-level interaction. When $R_c > 0.5 \text{ nm}$, the concentration quenching mechanism is due to a multi-level interaction.) When a single activator is incorporated into the matrix, the relationship between the luminous intensity of the sample and the concentration of the activator x is as follows:

$$\lg(I/x) = c - (\theta/3)\lg x \quad (5)$$

θ is a multilevel interaction function, and c is a constant. $n = 6, 8$, and 10 represent dipole–dipole, dipole–quadrupole, and quadrupole–quadrupole interactions, respectively¹⁶. The sample is excited by near-ultraviolet light at 378 nm with $x = 0.005, 0.01, 0.015, 0.02$. The relationship between $\lg(I/x)$ and $\lg(x)$ at 550 nm is shown in Fig. 4. It was found that the fitting slope is $-\theta/3 \approx -3.62$. Hence, $\theta \approx 10$, which corresponds to the electric four-level interaction.

Luminescence characteristics of $\text{KAlSiO}_4: 1.5 \text{ mol\% Tb}^{3+}, x \text{ mol\% Li}^+$ series samples. Figure 5a shows the UV–Vis absorption spectrum of the $\text{KAlSiO}_4: 1.5 \text{ mol\% Tb}^{3+}, x \text{ mol\% Li}^+$ ($x = 1, 1.5, 2$) series samples. It can be seen from the figure that this series of samples absorbs UV light well in the $250\text{--}400 \text{ nm}$ range. The strongest absorption peak at 249 nm is attributed to the charge transfer band transition (CTB) of Tb^{3+} . The absorption peak at 283 nm is due to the $4f^8 \rightarrow 4f^75d^1$ transition¹⁷. Weak absorption peaks appear at $352, 360$, and 378 nm , respectively. The characteristics of the absorption spectrum are consistent with those of the excitation spectrum of the $\text{KAlSiO}_4: 1.5 \text{ mol\% Tb}^{3+}$ sample. When $x = 1, 1.5$, and 2 , three absorption peaks are obtained in the wavelength range from $300\text{--}400 \text{ nm}$, all of which are typical $4f\text{--}4f$ electronic transitions of Tb^{3+} . When

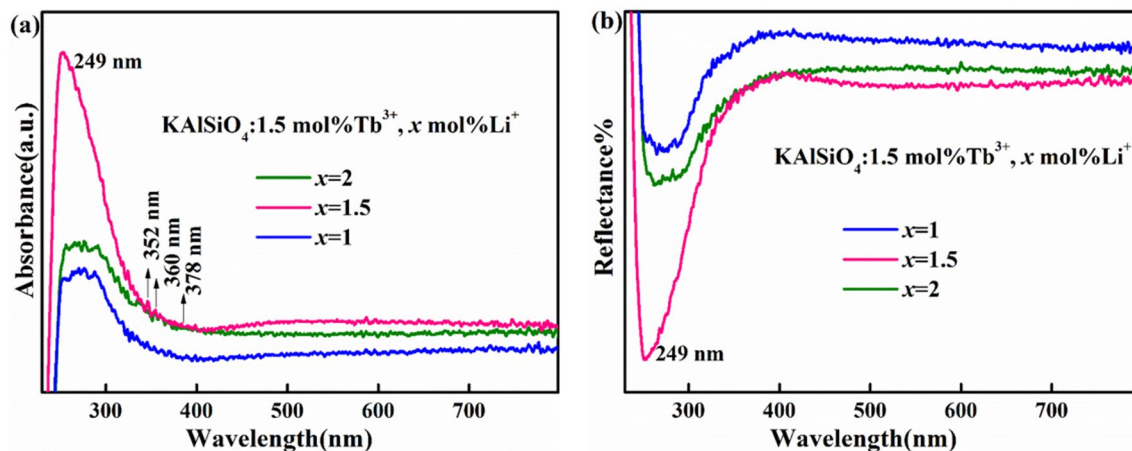


Figure 5. (a) UV-Vis absorption spectrum and (b) UV-Vis-NIR diffuse reflectance spectrum of $\text{KAlSiO}_4:1.5 \text{ mol}\% \text{Tb}^{3+}, x \text{ mol}\% \text{Li}^+$ series samples.

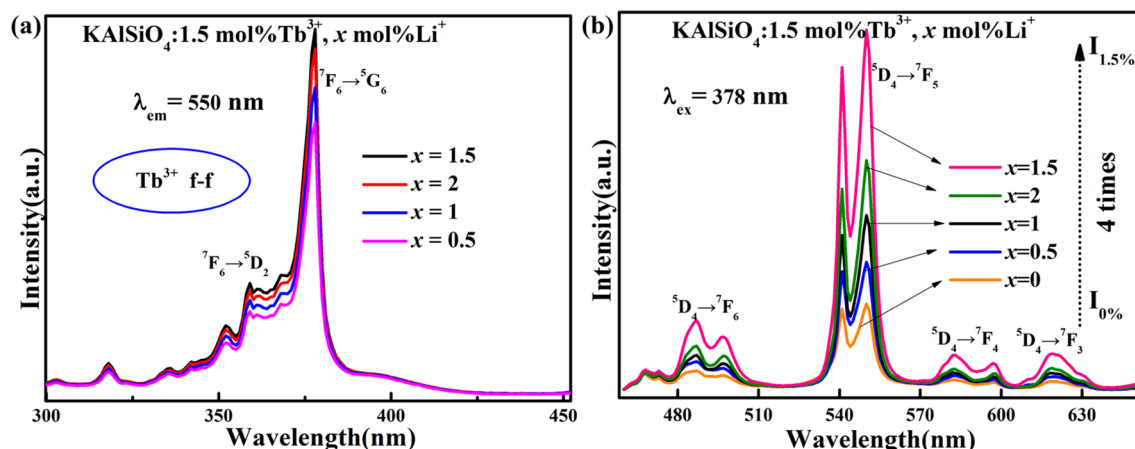


Figure 6. (a) Excitation spectrum and (b) emission spectrum of $\text{KAlSiO}_4:1.5 \text{ mol}\% \text{Tb}^{3+}, x \text{ mol}\% \text{Li}^+$ series samples.

$x=1.5$, the tangent of the absorption peak has the steepest slope. It shows that the $\text{KAlSiO}_4:1.5 \text{ mol}\% \text{Tb}^{3+}, 1.5 \text{ mol}\% \text{Li}^+$ sample shows the strongest absorption of ultraviolet light in the wavelength range from 250–800 nm. The excitation light of a commercial ultraviolet LED chip can effectively excite the sample. The strong absorption at 378 nm corresponds to the ${}^7\text{F}_6 \rightarrow {}^5\text{G}_6$ transition, and the other two weak absorptions at 352 nm and 360 nm originate from the ${}^7\text{F}_6 \rightarrow {}^5\text{D}_2$ and ${}^7\text{F}_6 \rightarrow {}^5\text{L}_{10}$ transitions, respectively. The results of UV-visible absorption spectroscopy showed that Tb^{3+} activator ions and Li^+ were successfully incorporated into KAlSiO_4 . This result is consistent with the XRD results.

Figure 5b shows the UV-Vis-NIR diffuse reflectance spectrum of the $\text{KAlSiO}_4:1.5 \text{ mol}\% \text{Tb}^{3+}, x \text{ mol}\% \text{Li}^+$ series samples. It can be seen from the figure that the sample has strong absorption in the wavelength range from 250–400 nm, and the sample with $x=1.5$ has the strongest absorption of ultraviolet and near-ultraviolet light. This result is consistent with the results of Figs. 3 and 5a. This further proves that this series of samples is suitable for excitation by white light LED chips. The strongest absorption peak at 249 nm is attributed to the 4f-5d charge transfer band transition of Tb^{3+} ion¹⁴. The absorption of the 4f-4f transition is weaker than that of the CTB transition.

Figure 6a,b shows the excitation spectrum and emission spectrum of the $\text{KAlSiO}_4:1.5 \text{ mol}\% \text{Tb}^{3+}, x \text{ mol}\% \text{Li}^+$ series samples. The excitation spectrum of this series of samples is obtained by monitoring with Tb^{3+} at 550 nm (${}^5\text{D}_4 \rightarrow {}^7\text{F}_5$). There are a series of excitation bands in the range of 300–450 nm, the main peaks are respectively 318, 352, 359, 378 nm, of which the strongest peak is at 378 nm. It confirms that it can be excited by ultraviolet light, near ultraviolet light and blue light.

It can be seen that as x increases, the intensity of the strongest emission peak at 550 nm (when excited with 378 nm) initially increases and then decreases. The best luminescence intensity is achieved when $x=1.5$ and is approximately 4 times the luminous intensity of the $\text{KAlSiO}_4:1.5 \text{ mol}\% \text{Tb}^{3+}$ sample, which can further prove that after Li^+ is added to the lattice, it promotes lattice matching. When $x=1.5$, the quenching concentration of $\text{KAlSiO}_4:1.5 \text{ mol}\% \text{Tb}^{3+}, x \text{ mol}\% \text{Li}^+$ can be obtained. At the same time, Li_2CO_3 can be used both as a charge compensation agent and as a flux. When Li_2CO_3 is used as a flux, Li^+ can modulate the valence of Tb^{3+} ions,

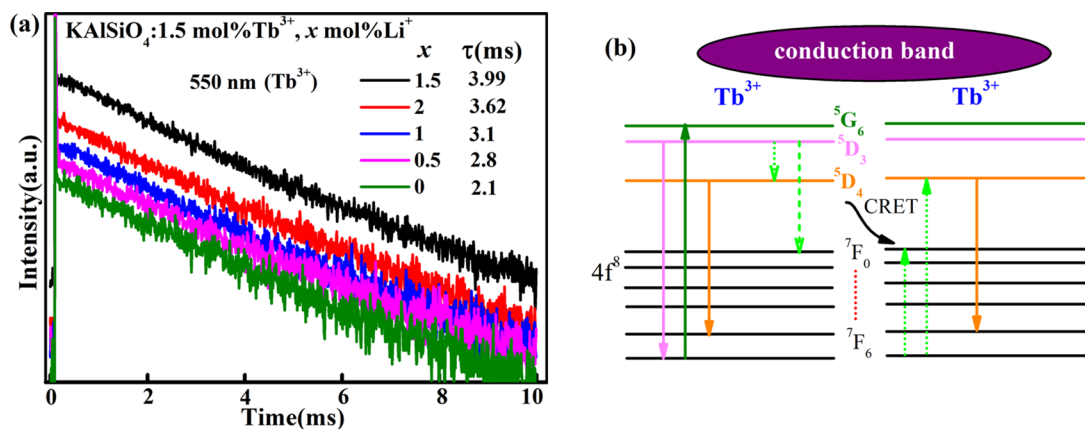


Figure 7. (a) Lifetime decay curves of $\text{KAlSiO}_4:1.5 \text{ mol\% Tb}^{3+}, x \text{ mol\% Li}^+$ series samples at 550 nm; (b) the energy level diagram of Tb^{3+} in KAlSiO_4 .

and it can contribute to the good light-emitting performance of the phosphor, that is to say, when the doping concentration of Tb^{3+} increases to 2 mol%, the luminescence performance of the sample is declined.

The substitution of K^+ with Tb^{3+} is an unequal valency substitution. Doping with a small amount of Li^+ can improve the lattice matching efficiency as it belongs to the same family as K^+ . This makes the cation charge in the crystal reach a relatively balanced state, thereby promoting the successful entry of Tb^{3+} into the K^+ lattice site, and greatly enhancing the luminous efficiency of the strongest emission peak. This result shows that the incorporation of Li^+ is beneficial for improving the luminous performance of the new $\text{KAlSiO}_4:1.5 \text{ mol\% Tb}^{3+}$ green-emitting phosphor. Hence, the $\text{KAlSiO}_4:1.5 \text{ mol\% Tb}^{3+}, 1.5 \text{ mol\% Li}^+$ green-emitting phosphor is expected to have higher luminous efficiency.

Figure 7a shows the lifetime decay curves of the $\text{KAlSiO}_4:1.5 \text{ mol\% Tb}^{3+}, x \text{ mol\% Li}^+$ series samples at 550 nm. It can be seen that as the Li^+ concentration increases, the Tb^{3+} lifetime gradually increases. When $x = 1.5$, the lifetime value reaches the maximum, which is 3.99 ms. This lifetime value is 2.45 ms longer than that reported in¹⁸. The lifetime decay curve is completely consistent with the emission spectrum shown in Fig. 6, indicating that for the KAlSiO_4 matrix, the best doping concentration of both Tb^{3+} and Li^+ is 1.5 mol%, which results in the highest luminous efficiency and the longest lifetime. It is suitable for use in white LED lighting. The lifetime value is calculated using Eq. (6)¹⁹:

$$\tau^* = \frac{A_1 \tau_1^2 + A_2 \tau_2^2}{A_1 \tau_1 + A_2 \tau_2} \quad (6)$$

Figure 7b shows the energy level diagram of Tb^{3+} in KAlSiO_4 . The energy transfer between Tb^{3+} - Tb^{3+} generally occurs in this way. For example, in this system, the excited state electrons will quickly relax to the lower $4f$ state, such as $^5\text{D}_3$, $^5\text{D}_4$, and then return to ground state.

Figure 8a, b shows the relationship between x and the FWHM and the integrated peak area at 550 nm for the $\text{KAlSiO}_4:1.5 \text{ mol\% Tb}^{3+}, x \text{ mol\% Li}^+$ series samples. It can be seen from the figure that when $x = 1.5$, the FWHM value is minimized, which is suitable for backlight LED lighting. The integrated peak area intensity reaches a maximum, which is consistent with the emission spectrum characteristics shown in Fig. 6.

Figure 9 shows the colour coordinates and body colour changes of the $\text{KAlSiO}_4:1.5 \text{ mol\% Tb}^{3+}, x \text{ mol\% Li}^+$ series samples. It can be seen that the colour coordinates of the samples do not change significantly with the increase in x . The colour coordinates of all the samples in the series are near the green region (0.33, 0.59), which preliminarily shows that the series of samples has good colour stability. The body colour of the sample gradually changes to deep green as x increases.

Table 1 shows the colour coordinates, colour purity, internal quantum yield (IQY), and colour temperature (CCT) of the $\text{KAlSiO}_4:1.5 \text{ mol\% Tb}^{3+}, x \text{ mol\% Li}^+$ series samples. It can be seen that the coordinates of all the samples are approximately (0.32, 0.56). The internal quantum yield is as high as 42%, the colour purity is as high as 83.3%, and the colour temperature of the samples is approximately 5500 K. The colour purity is calculated using Eq. (7)²⁰:

$$C_p = \frac{\sqrt{(x_s - x_i)^2 + (y_s - y_i)^2}}{\sqrt{(x_d - x_i)^2 + (y_d - y_i)^2}} \times 100\% \quad (7)$$

C_p is colour purity, $(x_d, y_d) = (0.3473, 0.65)$ is the international standard colour coordinate corresponding to the main wavelength of 550 nm, $(x_i, y_i) = (0.333, 0.333)$ is the colour coordinate of standard white light, and (x_s, y_s) is the colour coordinate of the series of samples. It can be seen from Table 1 that when $x = 1.5$, the sample colour purity is 83.3% and the quantum yield is 42%.

Figure 10 shows the emission spectrum of the $\text{KAlSiO}_4:1.5 \text{ mol\% Tb}^{3+}, 1.5 \text{ mol\% Li}^+$ when it is stored and exposed to air for 0, 10, 20, and 30 days. The relationship between the sample body colour and the number of

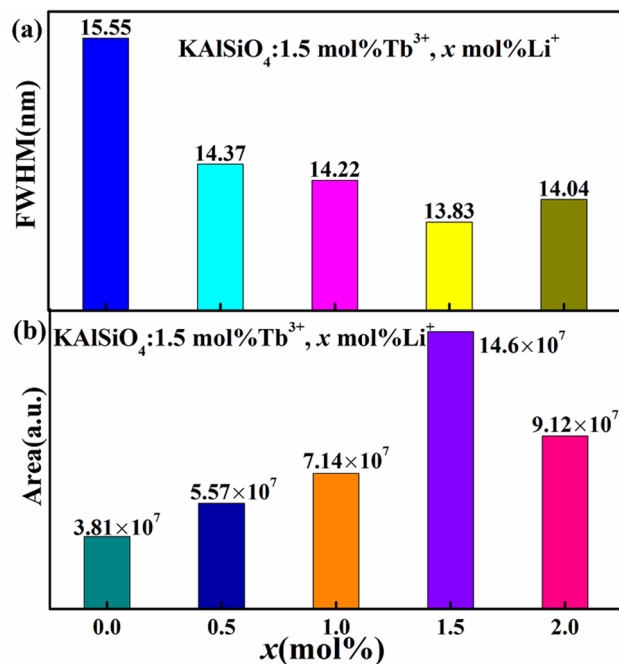


Figure 8. (a) Relationship between x and FWHM at 550 nm for KAlSiO₄: 1.5 mol% Tb³⁺, x mol% Li⁺ sample; (b) relationship between x and the integrated peak area at 550 nm for KAlSiO₄: 1.5 mol% Tb³⁺, x mol% Li⁺ sample.

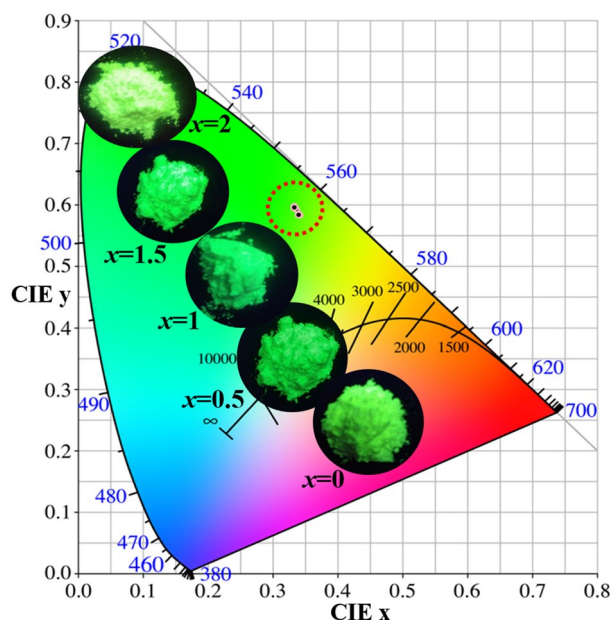


Figure 9. Colour coordinates and body colour changes of the KAlSiO₄: 1.5 mol% Tb³⁺, x mol% Li⁺ series samples.

storage days is also shown in the figure. It can be seen from the figure that the emission intensity is gradually weakened. However, the luminous intensity is reduced by half, and the sample main body colour still emits green light when irradiated with a 365 nm UV lamp. This further shows that the new green-emitting fluorescent phosphor has good stability and is suitable for the green component of the three-primary white LED.

The luminous performance of the phosphor suitable for white LED devices is generally determined by measuring the thermal stability of the phosphor. Figure 11 shows the variation of the intensity of the spectrum corresponding to KAlSiO₄: 1.5 mol% Tb³⁺, 1.5 mol% Li⁺ with temperature. It can be seen from the figure that when the temperature rises, the emission peak intensities of the phosphor at 550 nm at 50 °C, 100 °C, and 200 °C are 96.5%, 96%, and 95.1% at room temperature, respectively. This shows that the silicate phosphor has good

x	CIE(x, y)	C_p	CCT	IQY
0	(0.3399, 0.5838)	79.06%	5461	18%
0.5	(0.3417, 0.5839)	79.15%	5430	23%
1	(0.3359, 0.5927)	81.85%	5533	27%
1.5	(0.3327, 0.5974)	83.3%	5589	42%
2	(0.3331, 0.596)	82.8%	5582	35%

Table 1. Colour coordinates, colour purity, colour temperature, and internal quantum yield of $\text{KAlSiO}_4:1.5 \text{ mol \% Tb}^{3+}, x \text{ mol \% Li}^+$ samples.

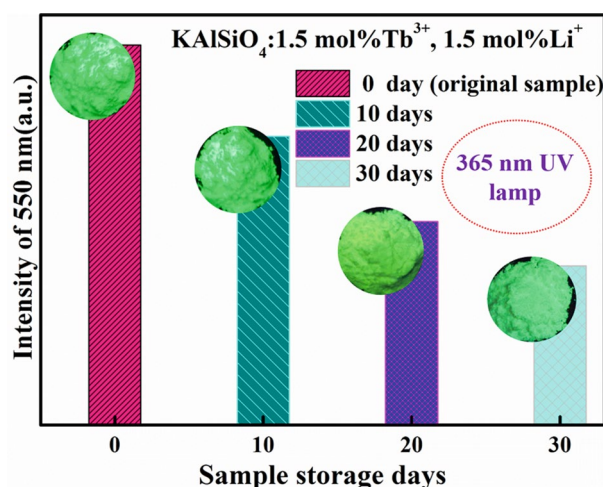


Figure 10. Variation of the emission peak intensity and sample body colour of $\text{KAlSiO}_4:1.5 \text{ mol \% Tb}^{3+}, 1.5 \text{ mol \% Li}^+$ with number of storage days.

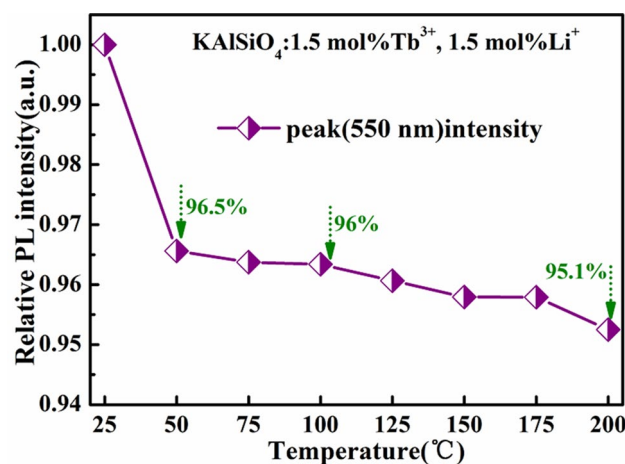


Figure 11. Variation of spectral light intensity of $\text{KAlSiO}_4:1.5 \text{ mol \% Tb}^{3+}, 1.5 \text{ mol \% Li}^+$ with temperature.

luminous efficiency and good thermal stability. This shows that the luminescence performance of the silicate phosphor has room for improvement. It is expected to be suitable for green phosphors in LED devices for a new generation of solid-state lighting.

Conclusion

We have prepared a new green-emitting phosphor, $\text{KAlSiO}_4:1.5 \text{ mol \% Tb}^{3+}, x \text{ mol \% Li}^+$ ($x=0, 0.5, 1, 1.5, 2$). The chemical structure of this series of samples is found to be highly stable. The doping of Tb^{3+} and Li^+ does not affect the crystal structure of the matrix. After the small-radius rare earth ions replace K^+ , the grain size

Chemical formula of raw materials	Purity	Production company
K ₂ CO ₃	99.99%	Shanghai Aladdin Biochemical Technology Co., Ltd
Al ₂ O ₃	99.99%	
SiO ₂	99.99%	
Tb ₂ O ₃	99.9%	
Li ₂ CO ₃	99.99%	

Table 2. Raw materials of KAlSiO₄: Tb³⁺, Li⁺ phosphor.

Experimental method	Test instrument name (or software name)
Phase analysis	Shimadzu XRD-6100 powder diffractometer
Photoluminescence spectrum (lifetime)	FLS920 Steady/Transient Fluorescence Spectrometer, Edinburgh, UK
Color coordinates	CIE1931
Internal quantum yield(IQY)	Hamamatsu C11347 absolute quantum efficiency tester
Thermal stability	Beijing (FJ-427A1) tester

Table 3. Instrument parameters and experimental methods used in this study.

decreases by 11.4% with an increase in the concentration of Li⁺ doping. The optimal doping concentration of Li⁺ in KAlSiO₄:1.5 mol% Tb³⁺ was found to be 1.5 mol%. When $x = 1.5$, the sample strongly absorbs the ultraviolet light in the range from 250 to 400 nm. The luminous intensity of the KAlSiO₄:1.5 mol% Tb³⁺ sample at 550 nm is increased by 4 times. The sample lifetime increased to 3.99 ms, the integrated peak area at 550 nm reached the maximum, and the full width at half maximum dropped to 13.83 nm. These results are closely related to the highly symmetrical crystal structure of the sample matrix. The colour purity of the sample series was found to be 83.3%. The body colour of the samples showed a little change with the increase in storage days. The samples exhibited good colour stability and thermal stability. The experimental results show that the developed phosphor is expected to become a candidate material for the green component of solid-state lighting white LEDs.

Experiment

Sample preparation and characterisation. KAlSiO₄:1.5 mol% Tb³⁺, x mol% Li⁺ ($x = 0.5, 1, 1.5, 2$) was prepared in an MF-1750C Beyke high-temperature box furnace by the high-temperature solid-phase method at 1350 °C for 210 min. The main raw materials used are listed in Table 2. The Li₂CO₃ can act as a flux, which contributes to the favorable properties of the KAlSiO₄:1.5 mol% Tb³⁺ phosphors in this work¹.

The quality of all the raw materials was calculated by the stoichiometric molar ratio method (mol%). The weighed materials were placed into an agate mortar and ground for 35 min. The uniformly mixed series of samples were placed into corundum crucibles and calcined in a high-temperature box furnace at a heating rate of 5 °C/min. After cooling the sample to room temperature, it was removed and ground again for the sample loading test.

The instrument parameters and experimental methods used in this study are presented in Table 3.

Received: 25 October 2020; Accepted: 10 February 2021

Published online: 04 March 2021

References

1. Yibo, C. *et al.* Localized charge accumulation driven by δ Li⁺ incorporation for efficient LED phosphors with tunable photoluminescence. *Chem. Mater.* **32**, 9551–9559 (2020).
2. Zhong, J. *et al.* Closing the cyan gap toward full-spectrum LED lighting with NaMgBO₃:₄Ce³⁺. *Chem. Mater.* **32**(2), 882–888 (2020).
3. Kaiheriman, M., Sidike, A., Maimaitinasier, A., Reheman, A. & Rouzi, B. Photoluminescence properties of Tb³⁺ doped sodalite under VUV–UV light excitation. *J. Lumin.* **157**, 411–415 (2015).
4. Ying, W. *et al.* Synthesis luminescence properties of a new type of green fluorescent powder BaAl₂Si₂O₈:Tb³⁺, Ce³⁺. *Spectrosc. Spect. Anal.* **37**(5), 1597–1602 (2017).
5. Yu, T., Wang, L., Yang, X., Ding, W. & Zhang, Q. The luminescence properties and thermal stability of a green-blue color tunable Sr₂SiO₄:Tb³⁺, Ce³⁺ phosphor. *Electron. Mater. Lett.* **15**(1), 18–26 (2017).
6. Halmurat, D., Taximaiti, Y., Wang, Q., He, J. & Sidike, A. Rare earth ion Tb³⁺ doped natural sodium feldspar (NaAlSi₃O₈) Luminescent properties and energy transfer. *Sci. Rep.* **9**(1), 14637 (2019).
7. Singh, V., Tamboli, S., Dhoble, S. J. & Jeong, H. Ultraviolet, vacuum ultraviolet excited photoluminescence study of sol-gel derived CaAl₂O₇:Tb³⁺ green emitting phosphor. *Optik*. **213**, 164375 (2020).
8. Zhen, L. *et al.* Luminescence properties of Sr₂MgB₂O₆:Tb³⁺, Li⁺ green-emitting phosphor. *J. Rare Earth.* **35**(3), 211 (2017).
9. Liang, J. K. *Determination of crystal structure by powder diffraction* 2nd edn, Vol. 77 (Science Press, Beijing, 2011).
10. Zhang, Z. *et al.* White light emission characteristics of Tb³⁺/Li⁺Sm³⁺ co-doped glass ceramics containing YPO₄ nanocrystals. *J. Mater. Sci. Technol.* **33**, 432–437 (2017).
11. Sheng, T. *et al.* Solvothermal synthesis and luminescence properties of BaCeF₅ and BaCeF₅: Tb³⁺, Sm³⁺ nanocrystals: An approach for white light emission. *J. Phys. Chem. C.* **116**(36), 19597–19603 (2012).

12. Abdallah, A. *et al.* Lanthanide-based coordination polymers with 1,4-carboxyphenylboronic ligand: Multiemissive compounds for multisensitive luminescent thermometric probes. *Inorg. Chem.* **58**(1), 462–475 (2019).
13. Li, M., Takei, T., Zhu, Q., Kim, B. & Li, J. Morphology tailoring of ZnWO₄ crystallites/architectures and photoluminescence of the doped RE³⁺ ions (RE = Sm, Eu, Tb, and Dy). *Inorg. Chem.* **58**(14), 9432–9442 (2019).
14. Biswas, P. & Kamni, V. K. The structural and spectral study of LiSrVO₄:Tb³⁺ phosphor for UV-shifted imaging devices. *Mater. Today Proc.* **28**(2), 1018–1023 (2020).
15. Wang, L. Fluorescence resonance energy transfer of CaF₂:Eu²⁺, Tb³⁺ applied to dye-sensitized solar cells. *Spectrochim. Acta A* **202**, 76–80 (2018).
16. Xian, J. *et al.* Synthesis and photoluminescence properties of Ln³⁺ (Ln³⁺ = Tb³⁺, Dy³⁺, Sm³⁺, Er³⁺)-doped Ca₂Nb₂O₇ phosphors. *Phys. B* **483**, 19–25 (2016).
17. Thomas, K. Energy transfer driven tunable emission of Tb/Eu co-doped lanthanum molybdate nanophosphors. *Opt. Mater.* **80**, 37–46 (2018).
18. Zhu, H. *et al.* Tunable luminescence and energy transfer of Tb³⁺/Eu³⁺ co-doped cubic CaCO₃ nanoparticles. *J. Lumin.* **203**, 441–446 (2018).
19. Miao, S., Hu, J., Gao, M., Zeng, J. & Kong, B. Tunable blue–green–emitting Na₄CaSi₃O₉:Ce³⁺, Li⁺, Tb³⁺ phosphor with energy transfer for near-UV white LEDs. *Mater. Today Sustainability*. **9**, 100036 (2020).
20. Zhu, J. *et al.* Structure–optical behavior correlation, optimized photoluminescence, and DFT calculation of La₇O₆(BO₃)(PO₄)₂:Sm³⁺ micropowder for solid state lighting. *ACS Appl. Electron. Mater.* **1**, 1688–1697 (2019).

Acknowledgements

This work was supported by the Scientific Research Projects of Universities in Xinjiang Autonomous Region (XJEDU2017I009); The Scientific Research and Innovation Project of postgraduates in Xinjiang Autonomous Region (XJ2020G233).

Author contributions

A.S. (First corresponding author): Corrected the academic errors in the manuscript. T.Y. (Second corresponding author): Correct the mistakes and improved the English grammar of manuscript. R.Y. (First author): Measured all the data of this manuscript, wrote this manuscript text. M.K. (Second author): Correct the mistakes in the experiment. All authors have reviewed this manuscript.

Competing interests

The authors declare no competing interests.

Additional information

Correspondence and requests for materials should be addressed to T.Y. or A.S.

Reprints and permissions information is available at www.nature.com/reprints.

Publisher's note Springer Nature remains neutral with regard to jurisdictional claims in published maps and institutional affiliations.



Open Access This article is licensed under a Creative Commons Attribution 4.0 International License, which permits use, sharing, adaptation, distribution and reproduction in any medium or format, as long as you give appropriate credit to the original author(s) and the source, provide a link to the Creative Commons licence, and indicate if changes were made. The images or other third party material in this article are included in the article's Creative Commons licence, unless indicated otherwise in a credit line to the material. If material is not included in the article's Creative Commons licence and your intended use is not permitted by statutory regulation or exceeds the permitted use, you will need to obtain permission directly from the copyright holder. To view a copy of this licence, visit <http://creativecommons.org/licenses/by/4.0/>.

© The Author(s) 2021